Caltech Submillimeter Observatory
Hiroko SHINNAGA
111 Nowelo St. Hilo, HI 96720 USA
California Institute of Technology (PMA)

Voice: +1 808 961 1909

Fax : +1 808 961 6273

Email: shinnaga@submm.caltech.edu

TECHNICAL MEMORANDUM

To:	Richard Chamberlin, Tom Phillips, Darren Dowell, Hiro Yoshida, Ruisheng Peng, CSO Staff
From:	Hiroko Shinnaga
CC:	CSO high frequency observers
Date:	November 22, 2004
Subject:	A Consideration of Thermal Effect on Pointing Measured on a Nasmyth Focus of the CSO 10.4m Leighton Telescope at $\lambda350\mu$m

ABSTRACT

Pointing data taken at $\lambda350$ μm using SHARCII during 31 August – 04 October 2004 were thoroughly examined and analyzed to improve the pointing of the telescope on a Nasmyth focus. The results clearly show that there is a temperature dependency on the pointing ($\sim -1''$shift per $+1$ degC change for both FAZO/FZAO axes over a temperature range of $-2 - +5$ degC). This technical memorandum summarizes the results and suggests that it would be useful to take the temperature into account for the pointing model of the telescope in future.

1 INTRODUCTION

Pointing is an important issue for large millimeter and submillimeter telescopes. The CSO telescope, located at 4200 m in the altitude, is a very unique telescope which covers the frequency bands from 180 up to 950 GHz. At the shortest wavelength, the beam size of the telescope becomes about $10''$, which is a typical beam width for the shortest operational wavelength for the telescopes. Pointing accuracy on a design goal sheet is normally set to be less than one fifth to one twentieth of the beam size (Ukita 1999). A pointing error of one fifth of a half-power beam width of a Gaussian beam causes a 10% of loss in sensitivity, which is significant for detection studies. Therefore, tracking accuracy and pointing repeatability of about two arcseconds or less is desirable for $10''$beam size (at the shortest operational wavelengths band).

SHARCII (Dowell et al. 2002), which was developed for the CSO telescope and is operational at $\lambda350$, 450, 850 μm, has an efficient imaging capability because it has a 384 pixels

two dimensional array. Combining with the unique scan modes such as Lissajous scan, Box scan, and sometime using chopping mode, SHARCII allows us to make a sensitive imaging at submillimeter wavelengths from ground. SHARCII images will give us two dimensional information from one scan, so that observers can correct pointing error when analyzing the data by adjusting the center. However, heterodyne receivers have only one beam so that repeatability of the pointing is more critical, especially when we try to detect very weak signal. And that is always the case for cutting edge sciences. Pointing error caused by instrumental alignment or gravitational deformation can be corrected by taking the effects into account for the pointing model because these effects are constant as far as the hardware stays the same. On the other hand, wind or temperature influences on the structure of the telescope in a relatively short time scale (less than 1 hour). To minimize these effects, the CSO telescope is placed in the dorm.

One of very unique points is that the CSO telescope has the dish surface optimization system (DSOS[1]) implemented by Leong et al. at the observatory (Leong et al. 2003). It allows us to make a gravitational deformation correction physically. The good performance improves the surface accuracy (from 25 to 13 μm) significantly. Accordingly, the efficiency at 850 GHz band has been improved from 33 % to 62 %, which is close to the theoretical capability of the telescope 66% (Leong et al. 2003). This DSOS is therefore a key component for very sensitive observations at the short submillimeter wavelength using the telescope.

In the SHARCII 2004 autumn run, observers took many pointing data. One would be able to examine the pointing stability in detail from the data accumulated during the period. Here the results of the pointing status (as of early October 2004) are summarized and discussed towards improving the pointing model.

2   THE DATA

Quite a lot of SHARCII pointing data were taken during the 2004 autumn run. In total, for both science and pointing, about 2400 images were taken during the entire run. Among them, λ350 μm pointing scans were extracted, which have a typical integration time of shorter than 200 seconds. For all the pointing scans, bright and compact sources, such as planets/massive asteroids (e.g., Uranus, Neptune, Vesta), evolved stars (e.g., AFGL 618, AFGL2688, OH231.8, omicron Cet), young stellar objects (HL Tau, L1551 etc), UCHII regions (e.g. W30H), and bright distant galaxy (ARP220), were used. CRUSH (Kovacs 2004) was used for data reduction. I filtered out the pointing scans when the DSOS (Leong et al 2003) was not working properly[2]. Also, pointing data taken with different pointing models[3] were filtered out for further analysis. All together, the data taken on Aug 31, Sep 1, 11 – 20, 25, 27, 28, Oct 3 – 4[4] were investigated. On Sep 14th, pointing model were changed for several times. So, the data taken with the original model were only extracted, according to the memo noted by Min[5]. Also, it should be note that the data sets were taken using two different reference pixels[6], namely (16.5, 6.5) and (16.5, 4.5). To compensate the positional difference, 9″was added to the FZAO values for the data whose reference pixel were (16.5, 4.5).

---

[1]For the latest information and the complete instruction to operate the system, please check the DSOS web site at http : //www.cso.caltech.edu/dsos/DSOS_MLeong.html

[2]Based on the DSOS logs, with great help from Melanie.

[3]Based on Darren's memo, received on Sep 19 by email.

[4]Date and time given in this memo are based on UT time.

[5]Based on Min's log on the night, received by email through Darek on Sep 14

[6]There were other data which used very different reference pixels. But they were filtered out.

The initial pointing parameters during the period were as follows;
- Constant terms[7]
YPOS_OFFSET = 0.30
YPOS_A = 3.97622
YPOS_B = 7.39625
XPOS_DESTINATION = -10.8
FOCUS_OFFSET = 0.00
FOCUS_A = 0.04570
- T Terms[8]:
TAZOF_A = 0.00
TAZOF_B = 2.70061E-5
TAZOF_C = 3.005845E-6
TZAOF_A = 0.00
TZAOF_B = -6.69182E-4
TZAOF_C = -6.593466E-6

Note that, during the period of Sep 20 – 22 (UT) 2004, the DSOS was left turned on for three days and nights. (Because of the reason, next observers on Sep 23 could not use the DSOS function unfortunately, since the system needed time for cool down.) This made the pointing behavior very unusual. Accordingly, the data taken during Sep 21 through 24 were not used for further analysis.

It is very important for the DSOS to be turned off when not used. It uses the temperature sensors to control the shape of the main dish (Leong et al. 2003). Because of the big temperature differences between day time and night time, the DSOS cannot be functional if the system is kept on for days and nights. It uses thermal electric cooler system to control the temperature. It needs to take a rest in day time to achieve the best performance in the night when the observations are done. Observers who have any question about the system are encouraged to contact Melanie or any CSO staff. In order to achieve our best results at the highest frequencies, the DSOS is a key instrument.

Figure 1 shows the sky coverage of the pointing data. Note that, at the CSO telescope, we use azimuth range from −90 to 360 degrees, due to a spiral motion of azimuth bearing which was suspected around seven years ago (Yoshida, private communication). In the pointing model, there is the azimuth terms for the pointing correction and this azimuth range is used (Yoshida 1997). Accordingly, although Az = 270 and −90 corresponds the same direction (namely west[9]), here we present the results in the same manner, for convenience in comparison. Figure 1 also tells us that the pointing sources were limited in a certain sky area.

In the sky coverage diagram, there is a point at the very high elevation (almost 90 deg). Figure 2 left image is the one that was taken at the highest elevation at 88.6 deg. As you see there, the sidelobes are very significant. On the other hand, Figure 2 right image is taken at

---

[7]FAZO, FZAO values in the constant terms were changed for a couple of times. However, since they don't affect the first and second order terms, which are derived from least square fitting, these are not noted here. The fitting results are presented in next section.

[8]The unit for first and second order T terms are (radian per radian) and (rad/rad^2), respectively. When converting from arcsec per degree and from (arcsec per deg^2) to the above units, one needs to multiply $1/3600$ and $(180/\pi/3600)$ for first and second order terms, respectively(see also next section).

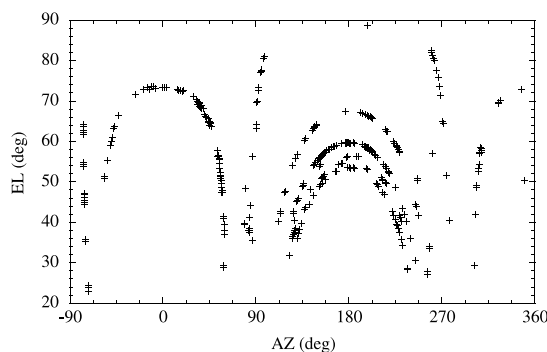[9]Az = 0 and 360 corresponds to north, as usual.

Figure 1: The sky coverage of the pointing data presented in this memo.

modest elevation (57.5deg). When both images were taken, the DSOS was working. It is hard to make a gravitational deformation correction at the highest elevation even with the DSOS. Since the pointing offsets of the high elevation data were quite different from the other offsets taken at reasonable elevations, as expected, and since the offsets affect significantly when making a fitting to examine the elevation dependency, this data was not used. Usually, it is not recommended to observe at high elevation (around 82-83 deg or higher), because it's getting harder for the telescope to track the objects and because of the beam shape.
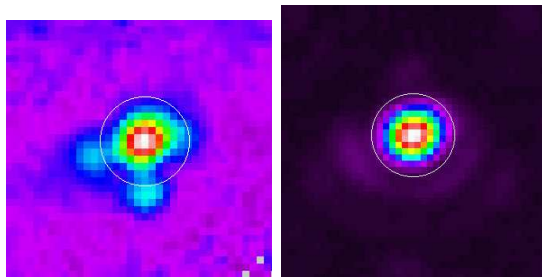
Figure 2: Images taken at the highest EL = 88.6 (left) and at modest EL (right) with SHARCII.
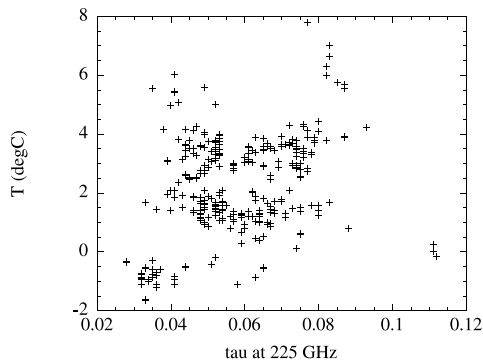

Figure 3: Tau measured at 225GHz – ambient temperature diagram. There is no strong correlation, but freezing temperature give us the best tau condition for most of the cases (see text).

Because of the requirement when use SHARCII, all the data were taken under tau at 225 GHz ~ 0.1 or less. In Figure 3, one can see that there is no strong correlation between ambient temperature[10] and tau at 225 GHz. However, cold weather below 0 degC always gives us the lowest tau condition, which makes sense considering the fact that water vapor freezes out at a temperature of below 0 degC.

---

[10]Measured at the top of the dorm.

3   RESULTS AND DISCUSSION

3.1   Overall Tendency on the AZ/EL Axes

Figure 4 shows the elevation dependency in the FAZO and FZAO offsets. One can see the general trend in both diagrams. Considering first and second order terms, one can make a fitting to find the best parameters for T terms. Namely, the fitting was made using the equation;

$$\text{FAZO or FZAO} = \text{M0} + \text{M1} \times \text{ZA} + \text{M2} \times \text{ZA}^2 \tag{1}$$

Note that we use the unit for FAZO and FZAO in arcseconds and the unit for EL in degrees. M0, M1, and M2 correspond to constant, first order, and second order terms, respectively. One can make a least square fitting to derive the solutions for each term and add the numbers in the current T terms, which were given in the previous section. One can see elevation dependency in both FAZO and FZAO, as shown in Figure 4. Closely looking the data, it turned out that the data taken on Aug 31 shows excessive scatters compared to the others. Because of the reason, the data were not used for detail analysis.
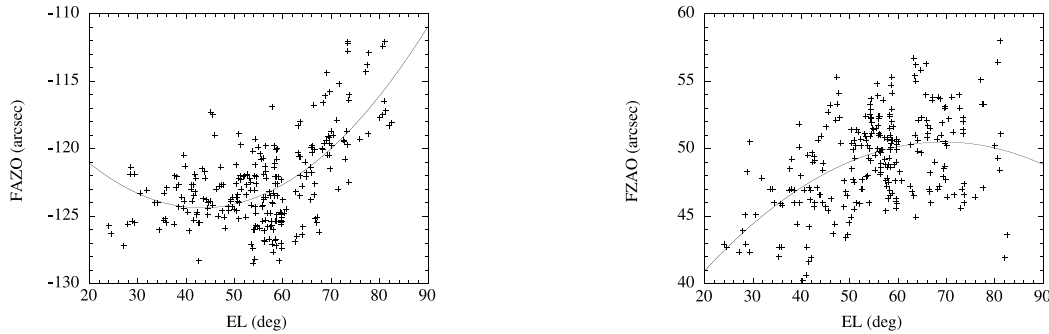

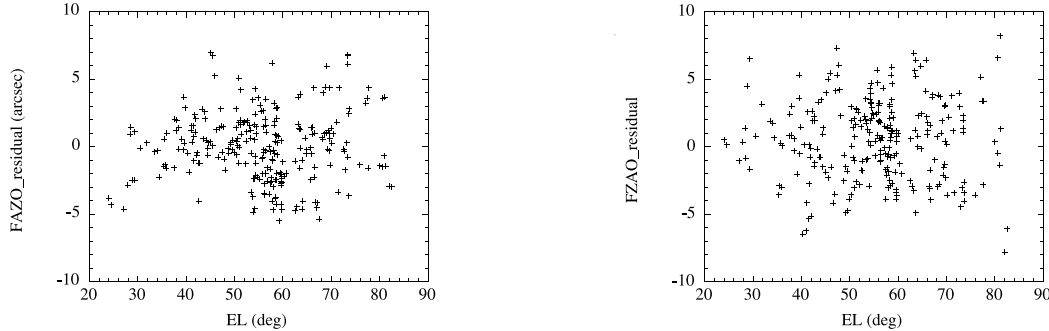Figure 4: FAZO-EL (left) and FZAO-El(right) plots.

Figure 5: Residuals from the fittings in FAZO (left) and in FZAO (right) vs. El diagrams

Figure 4 show the plot with the fitting curves. The least square fitting derived the following solutions for each term:

M0 (FAZO) = -110.9 ± 1.0   ; M0 (FZAO) = 48.8 ± 1.8
M1 (FAZO) = -0.575 ± 0.057   ; M1 (FZAO) = 0.162 ± 0.10
M2 (FAZO) = +0.0061 ± 0.00079 ; M2 (FZAO) = -0.0039±0.001

Figure 5 show the residuals subtracted the fitting model. The dispersions on the FAZO and FZAO residuals were $6.3''$ and $8.5''$, respectively. The RMS were $2.5''$ and $3.0''$ for FAZO and FZAO, respectively.

Figure 6 shows the azimuth dependency on the FAZO and FZAO. There is no strong dependency, although there might be some correlation. We shall neglect the azimuth term for now. In the last subsection of this section, the azimuth dependency issue will be revisited.
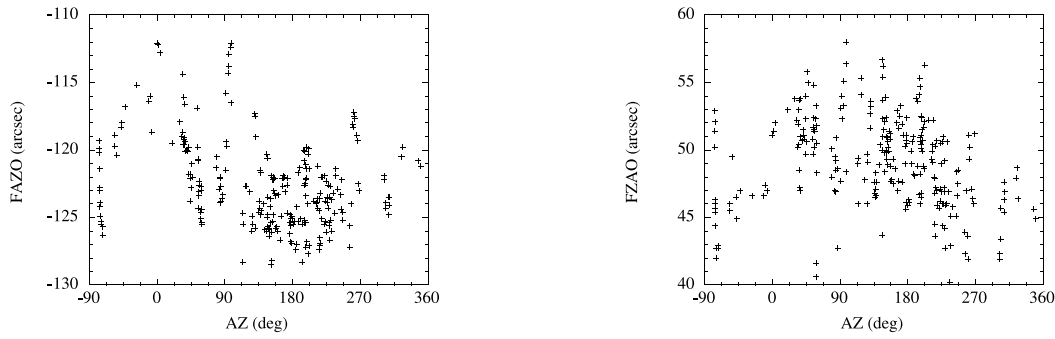
Figure 6: FAZO vs AZ (Left) and FZAO vs. AZ (right) plots.
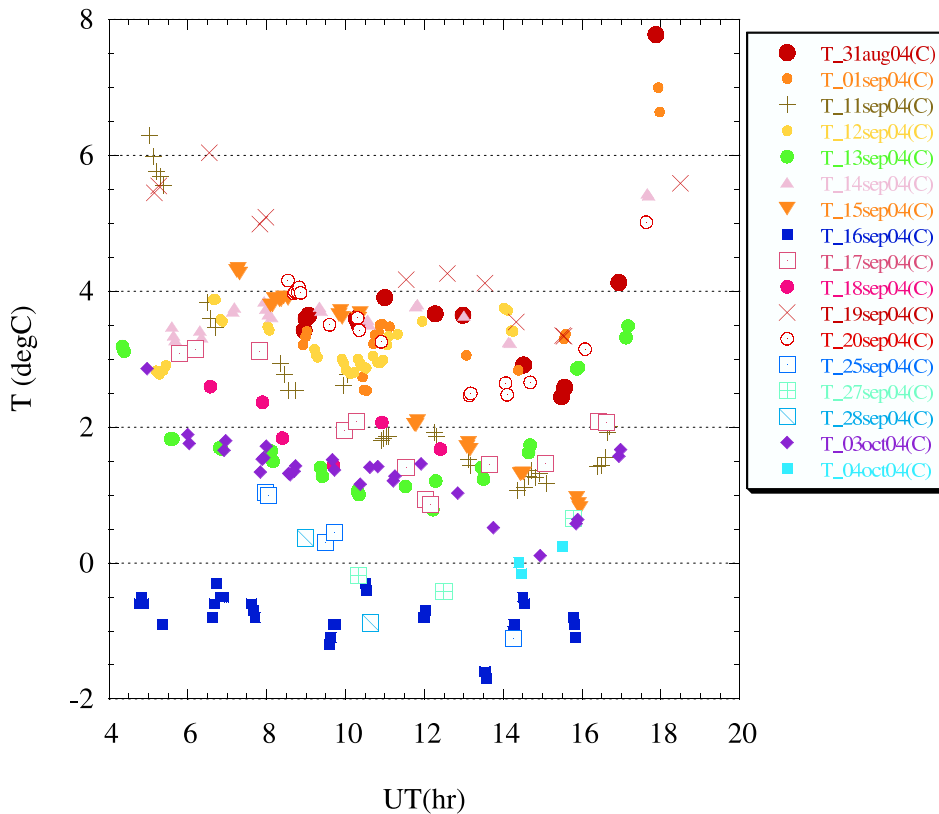
3.2 Thermal Effect

Figure 7: Ambient temperature changes during the observing runs.

Figure 7 shows the ambient temperature changes measured at the top of the dorm during the observing runs. One can see that temperature is more or less stays similar for most of cases, except for the time periods when observers started observation early (before 6h) before sunset, and when observers kept observations even after the Sun rises (around 17h and later). On Sep 11, there was the biggest gradient in temperature (the temperature difference between the max and the min was 5.2 degC) among the sample, while there was only 1.1 degC change in temperature on Sep 16th (the best weather condition among the sample).

Since the temperature could affect the pointing, the thermal dependency was investigated. Figure 8 shows the FAZO/FZAO – EL diagrams with colors to identify behavior of each night. One can clearly see that pointing deviations were much smaller if we consider one night only.

Also, these figures clearly tell us that the deviation becomes smaller when the temperature is lower (e.g., compare blue filled squares (Sep 16) and red filled circle (Aug 31).
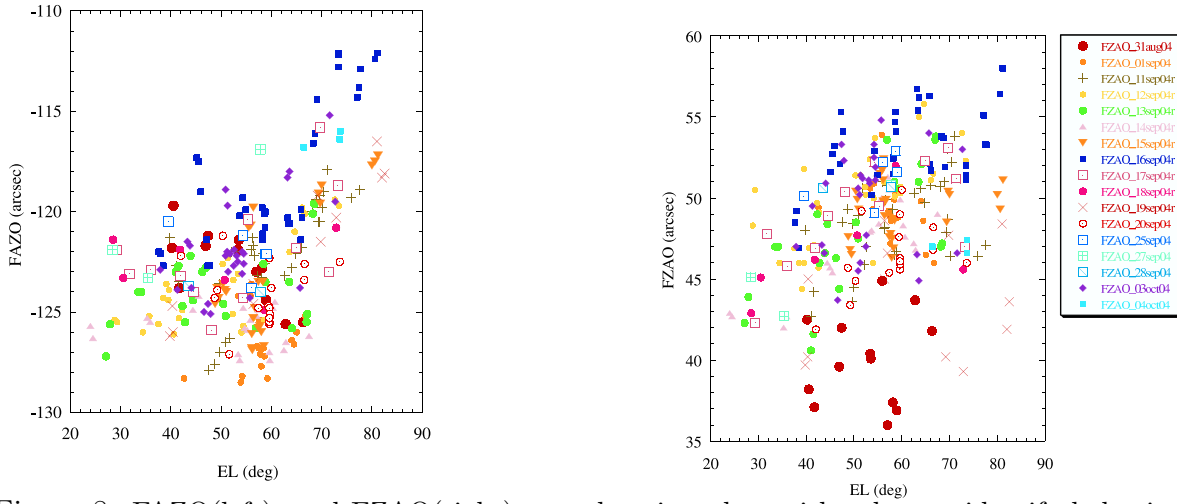

Figure 8: FAZO(left)- and FZAO(right)- vs. elevation plots with colors to identify behaviors of each night.

Since there is no correlation between ambient temperature and elevation, one can make a independent fitting for temperature.
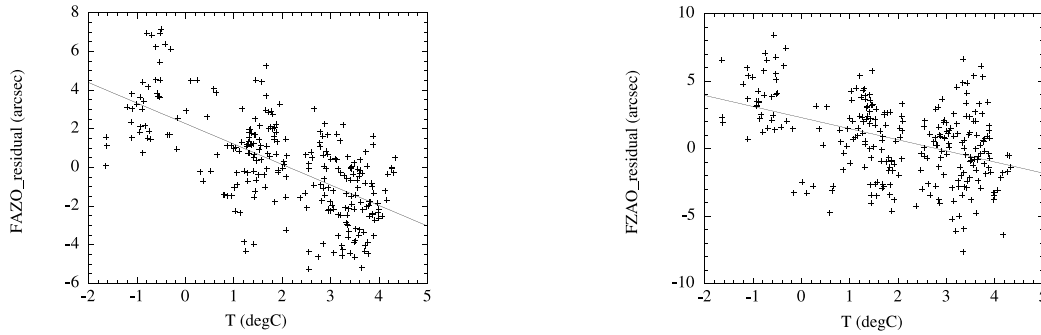

Figure 9: Ambient temperature vs. $\text{FAZO}_{residual}$(left) and $\text{FZAO}_{residual}$(right) diagrams.

Figure 9 show FAZO/FZAO vs. the ambient temperature diagrams. One can clearly see the strong linear correlations for both offsets. Here we applied first order correction only and found the following coefficients were derived for the constant and linear terms;

$\text{FAZO}_{residual} = (2.2 \pm 0.2) - (0.993 \pm 0.078) \times T$
$\text{FZAO}_{residual} = (2.3 \pm 0.3) - (0.99 \pm 0.11) \times T$

where T is ambient temperature, $(\text{FAZO/FZAO})_{residual}$ is the residual derived in the previous subsection, after elevation dependency correction.

This equation means that there is about -1 arcsecond change as 1 degC temperature changes, for both AZ and EL axes. Related issue is discussed in the next subsection.

Figure 10 and 11 shows the residuals vs. EL and ambient temperature after the thermal effect is subtracted. Figure 11 also indicate that, at higher temperature, the scatter of pointing becomes larger in FZAO (EL direction), especially above 3 degC, which is consistent with the fact that we saw from the Figure 8. For FAZO, there is no scatter difference as a function of ambient temperature. After taking the thermal effect into account, the dispersions for the FAZO
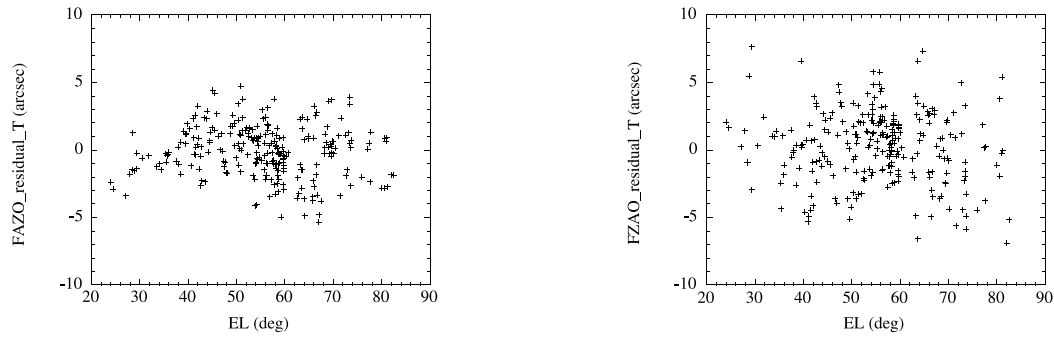
Figure 10: FAZO$_{residualT}$ (left)- and FZAO$_{residualT}$ (right)- EL diagrams.
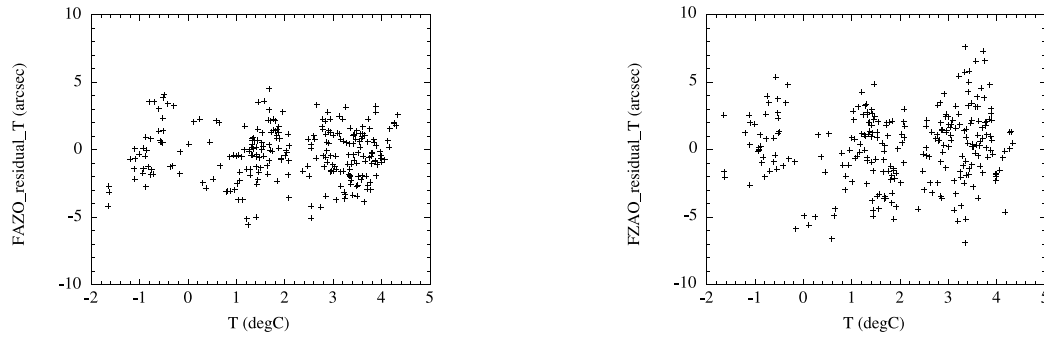
Figure 11: FAZO$_{residualT}$ (left)- and FZAO$_{residualT}$ (right)- ambient temperature diagrams.

and FZAO was improved to be $3.6''$(from $6.3''$) and $6.9''$(from $8.5''$), respectively. The RMS for FAZO/FZAO went down to $1.9''$(from $2.5''$) and $2.6''$(from $3.0''$), respectively.

3.3   Implications from The Thermal Effect

Chamberlin (2003) made temperature measurements at different places (bottom, middle and top of the main dish) on the backup structures of the CSO telescope. He reported significant temperature difference between top and middle positions over different elevations. The difference becomes larger at lower elevation and changes as a function of elevation. On a night when the T_{ant} was -2.2, the gradient of temperature difference was measured to be about 0.081 degC per 1 deg in Elevation, from EL 15 to EL 65. On the other hand, on a night when T_{ant} was -0.18, the gradient of temperature difference was measured to be about 0.072, from EL 30 to EL 65. The temperature difference became zero at EL $\sim$ 65 for both cases. On the other hand, there was no temperature gradient detected in left/right direction. This would cause main dish deformation (in EL axis) and continuous pointing shift over wide elevation range. And this must be closely related to the temperature dependency, about -1 arcsec per 1 degC, in both FAZO and FZAO axes, over EL $\sim$ 25 – $\sim$ 85 degrees, which we saw in the previous subsection. In addition to the main dish, the secondary structure may be also affected by the thermal effect.

3.4 Azimuth Dependency

After elevation and temperature corrections are made, dependencies to AZ, which seemed to be weaker before, becomes of interest. The correlation diagrams of AZ vs FAZO/FZAO residuals after elevation/temperature correlation were subtracted are made and shown in Figure12.
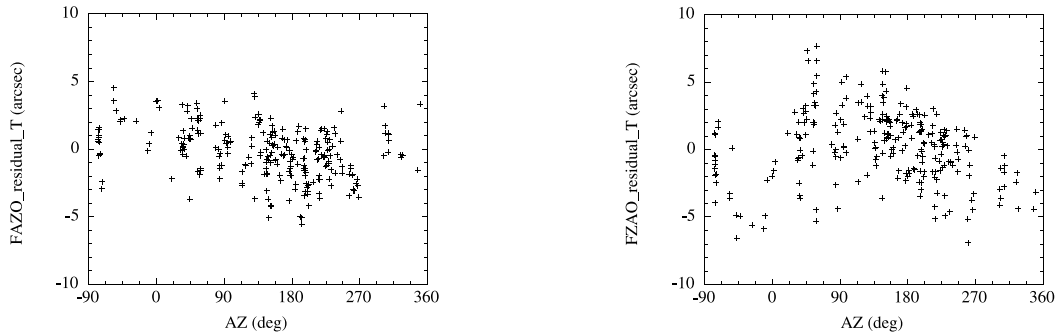

Figure 12: AZ vs. $\mathrm{FAZO}_{residualT}$ (left) and $\mathrm{FZAO}_{residualT}$ (right) (after elevation/temperature correction) diagrams. AZ range is plotted from -90 to 360 deg.

Figure 12 inspired me to change the range of azimuth from zero to 360 degrees, instead of -90 to 360deg. The diagrams of AZ vs FAZO/FZAO are made and shown in Figure 13 in Az from 0 to 360 deg.
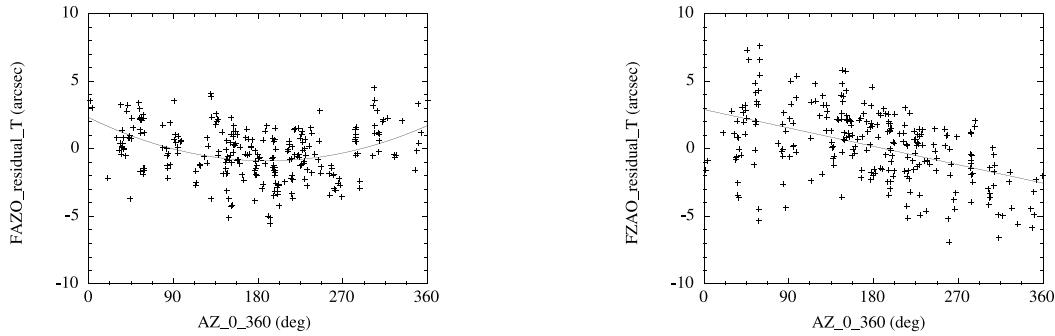

Figure 13: AZ (ranges from 0 – 360) vs. $\mathrm{FAZO}_{residualT}$ (left) and $\mathrm{FZAO}_{residualT}$ (right) diagrams.
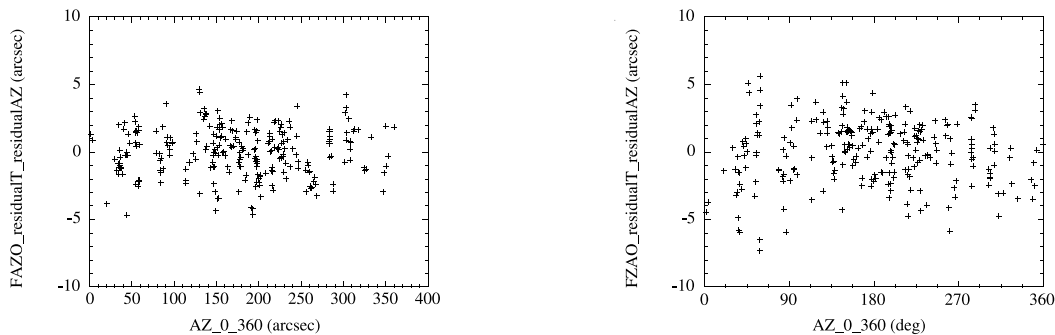

Figure 14: Final residuals in FAZO(left)/FZAO(right) after EL, temperature, AZ corrections.

The least square fitting (Figure 13) derived the following solutions for each case:
$\mathrm{FAZO}_{residualT}$=(2.3±0.4) $-$(0.034 ±0.005)×AZ + (8.9658E-5±1.3601E-5)×AZ^2
$\mathrm{FZAO}_{residualT}$=(2.9±0.3) $-$ (0.015±0.017)× AZ

There is a clear tendency that the FAZO has a minimum at AZ = 180 deg (namely, south). For FZAO, it seems there is a slight slope over the AZ range. But this is not significant, as one

can see from the fitting results. This might be related to the spiral motion (see Section 2) or may be due to some residuals left by optical pointing corrections[11].

Finally, the RMS for FAZO and FZAO were decreased down to $1.8''$(from $2.5''$with EL correction) and $2.3''$(from $2.9''$with EL correction), respectively. The dispersions are $3.0''$for FAZO (originally $6.3''$after elevation correction only) and $5.3''$(originally $8.5''$, after elevation correction) for FZAO, respectively.

4   SUMMARY

Thanks to the efficient imaging capability of SHARCII, mounted on a Nasmyth focus, over 360 pointing images taken at $\lambda 350\mu$m during 2004 autumn run were thoroughly examined and analyzed to investigate the pointing accuracy of the telescope. Considering the thermal effect, in addition to EL and AZ dependencies, it is possible to improve the pointing accuracy of the telescope down to $\sim \pm 2''$level, which is close to the theoretical limit of the telescope.

References

[1] Richard Chamberlin 2003, Surface Memo No.2, entitled "Temperature measurement on the Leighton Telescope"

[2] Darren Dowell et al. 2002 SPIE paper, entitled "SHARCII: a Caltech Submillimeter Observatory facility camera with 384 pixels"

[3] Attila Kovacs 2004, CRUSH manual, entitled "The CRUSH Approach to Data Reduction"

[4] Melanie Leong et al. 2003 AMOS conference paper entitled "Dish Surface Optimization System –Surface Correction on a 10.4 Meter Leighton Primary Mirror"

[5] Nobuharu Ukita 1999, Publ. Natil. Astron. Obs. Japan Vol. 5. 139 - 147, entitled "Thermal Effects on the Pointing of the Nobeyama 45-m Telescope"

[6] Hiroshige Yoshida 1997, Technical memo, entitled "Pointing Correction at the CSO"

---

[11]Comments from Richard, on 22 Nov 2004.